Journal of Hazardous Materials 369 (2019) 116–124

Contents lists available at ScienceDirect

Journal of Hazardous Materials

journal homepage: www.elsevier.com/locate/jhazmat

Effects of pool size and spacing on burning rate and flame height of two square heptane pool fires

Huaxian Wan[a], Zihe Gao[a], Jie Ji[a,b,*], Yongming Zhang[a], Kaiyuan Li[c], Liangzhu Wang[d]

[a] State Key Laboratory of Fire Science, University of Science and Technology of China, JinZhai Road 96, Hefei, Anhui 230026, China
[b] Institute of Advanced Technology, University of Science and Technology of China, Hefei, Anhui 230088, China
[c] Université Lille Nord de France, ENSCL, UMET/ISP R2Fire, Cité Scientifique-Bât C7-BP 90108, 59652 Villeneuve d'Ascq Cedex, France
[d] Department of Building, Civil and Environmental Engineering, Concordia University, 1445 de Maisonneuve Blvd. West, Montreal, QC H3G 1M8, Canada

ARTICLE INFO

Keywords:
Multiple pool fires
Flame height
Burning rate
Air entrainment
Heat feedback

ABSTRACT

The interaction of multiple pool fires might lead to higher burning rate and flame height than single pool fire, raising the possibility of fire ignition and flame spread and increasing the risks to people, buildings and environment. To quantify the burning rate and flame height of multiple pool fires from the view of physical mechanism, this paper presents an experimental study on two identical square pool fires. Heptane was used as fuel. The pool size and spacing were varied. Results showed that both the burning rate and flame height change non-monotonically with spacing. From the view of air entrainment, a correlation for the flame height of two pool fires is developed involving pool size, spacing and the flame height of zero spacing. The comparison with experimental results shows that the developed correlation is suitable for two heptane or propane fires. A theoretical study based on energy balance at one of the pool surfaces is performed to evaluate the burning rate of two fires, which is finally expressed as a function of pool size, spacing, burning rate and the flame height of single fire. The proposed model is validated using the experimental and literature data, which presents a reasonable reliability.

1. Introduction

Pool fires are the most frequent of process industry accidents [1,2]. The fuel mass burning rate and flame height are two of the most important topics of pool fires and both of them have been studied for decades [3–5]. Compared to elaborate and extensive studies on single pool fires, much less attention has been paid to multiple pool fires, which is usually termed as the interactively burning of two or more adjacent pool fires [1]. A domino effect could be formed once a fire is propagated from one pool to another [6]. When the fires are located sufficiently close, the restriction of air entrainment will lead to a pressure drop between fires, resulting in flames tilt to each other and even merge together [7]. The interaction of multiple flames might cause increases of burning rate and flame height when compared to a single flame [8]. The enhanced heat feedback to the fuel and flame outward radiation due to interaction raise the possibility of fire ignition and flame spread. To better understand the flame interaction intensity and flame radiation property, the information of burning rate and flame height of multiple pool fires is necessary.

The burning rate of pool fires is dependent on the heat transfers from the pool rim and flame to the fuel, including conduction, convection and radiation [9]. Four regimes of dominant heat transfer mechanism were reported by Hottel [10]: the conduction dominated regime for small pool diameters $D < 7$ cm, the transition regime from conduction to convection ($7\text{ cm} \le D < 10\text{ cm}$), the convection dominated regime for $10\text{ cm} \le D < 20\text{ cm}$ and the radiation dominated regime for $D \ge 20$ cm. For the single pool fire, the burning rate decreases with increasing D in the convection dominated regime, while it increases with D in the beginning and then maintains unchanged in the radiation dominated regime [11]. Based on this law, different correlations for the burning rate of single pool fires were proposed under different fuels and scales [11,12]. However, the spacing is provided as an additional important factor influencing the burning behavior of multiples pool fires [9,13–15]. In the study of Huffman et al. [9], the multiple pool fires were arranged in a circular array, i.e., one pool located in the center and the other pools placed around the center pool. Liu et al. [13–15] performed a series of experiments to study the burning rate of multiple pool fires in an $N \times N$ ($N = 3$–15) square array. It was found that the burning rate of multiple pool fires with luminous flames increases first and then decreases with decreasing the

* Corresponding author at: State Key Laboratory of Fire Science, University of Science and Technology of China, JinZhai Road 96, Hefei, Anhui 230026, China.
E-mail address: jijie232@ustc.edu.cn (J. Ji).

https://doi.org/10.1016/j.jhazmat.2019.01.111
Received 9 October 2018; Received in revised form 29 January 2019; Accepted 31 January 2019
Available online 05 February 2019
0304-3894/

Nomenclature

a	Parameter in Eq. (17)
A_f	Flame surface area (m^2)
D	Pool diameter/length (m)
F	Geometrical view factor
g	Gravitational acceleration (m/s^2)
h	Convective heat transfer coefficient ($kW/(m^2K)$)
ΔHc	Heat of combustion (MJ/kg)
ΔHg	Heat of gasification (kJ/kg)
I_f	Flame intermittency
L_f	Mean flame height above the pool surface (m)
$L_{f,S=0}$	Flame height with zero spacing (m)
$L_{f,S>0}$	Flame height with non-zero spacing (m)
$\dot{m}$	Burning rate of each pool (g/s)
$\dot{m}''$	Burning rate per unit area of each pool ($g/(m^2s)$)
$\dot{Q}$	Heat release rate of each pool (kW)
$\dot{q}_c''$	Convective heat flux received by the pool (kW/m^2)
$\dot{q}_r''$	Radiative heat flux received by the pool (kW/m^2)
$\dot{q}_{r,A-A}''$	Radiation received by pool A from its own flame (kW/m^2)
$\dot{q}_{r,B-A}''$	Flame radiation emitted by pool B and then received by pool A (kW/m^2)
S	Pool edge spacing (m)
T_∞	Ambient temperature (K)
T_f	Flame temperature (K)
ΔT_{add}	Temperature rise in the additional region (K)
U_f	Airflow velocity (m/s)
W	Flame width (m)

Greek symbols

ε	Flame emissivity
λ	Parameter in Eq. (1)
σ	Stephan-Boltzmann constant ($W/(m^2K^4)$)
χ_{rad}	Flame radiative fraction

Subscript

A	Pool A
B	Pool B
MF	Multiple fires
SF	Single fire

spacing [9,13]. Similar trend of burning rate against spacing was found by Ji et al. [16] for the investigation of two parallel pool fires located in a tunnel and also by Fan and Tang [17] for the study of two parallel pool fires under different wind velocities. Liu et al. [13] attributed the non-monotonic trend as a result of the competition between the heat feedback enhancement and the air entrainment restriction. When multiple pool fires are close to each other, the fuel surface of each pool receives the heat feedbacks not only from its own flame but also from the neighborhood flames, the enhanced flame heat feedback will promote the fuel evaporation and thus increases the burning rate [13]. Oppositely, the restriction of air entrainment reduces the combustion efficiency and thus weakens the heat feedback to fuel surface, resulting in a decrease of burning rate [13]. Despite the deep understanding of burning mechanisms, a viable correlation for predicting the burning rate of multiple pool fires from the view of physical mechanism is limited in literatures. This work aims to bridge the knowledge gap.

Along with the burning rate, the flame height of multiple pool fires will be inevitably affected by the interaction of flames. Former studies [17–22] have been measured the flame height of two fires in a parallel array in free space. Fan and Tang [17] experimentally obtained the flame height of two square heptane pool fires. Li and Liu [18] experimentally measured the flame height of two circular heptane pool fires. Vasanth et al. [19] measured the flame height of two circular heptane pool fires using the method of numerical simulation. Other than the liquid fuel, Sugawa and Takahashi [20], Wan et al. [21] and Tao et al. [22] measured the flame heights of two rectangular propane gas fires. Other than free space, the flame height or length from two fires in confined spaces was studied by Wan et al. [23,24]. Empirical correlations for the flame height were proposed in Refs. [17,20], while these correlations are usually isolated from the other experimental data. In our former work [21], a correlation for the flame height of two identical propane gas fires was developed and validated using both experimental and literature data. However, there is no unified correlation for flame heights of different fuel types, which motivates the present study.

Due to the complicated effect of air entrainment and heat feedback on multiple pool fires, one approach to establish desirable models of flame height and burning rate was to first use gas fires of which the heat feedback was not an important factor controlling the burning and then consider the influence of heat feedback separately [25]. Based on this research idea, the quantitative effect of air entrainment on flame height of two propane gas fires have been investigated in our previous work [21]. As a successive and systematic work, the effect of heat feedback on burning rate of multiple pool fires will be studied in depth through this work.

Therefore, this paper aims to study the burning rate and flame height of two identical heptane pool fires. The square pool size and edge spacing were changed. Correlations for flame height and burning rate of two identical fires were proposed from the view of physical mechanism. The comparison of calculated and experimental data in this work and literatures validated the accuracy of the proposed correlations. The current study can improve the understanding of interaction mechanisms of multiple pool fires and provide viable analytical methods for researchers to study the flame height and burning rate of multiple pool fires. A further aim of this paper is to provide experimental data for the validation of numerical simulations.

2. Experiments

Fig. 1 shows the experimental setup. Two identical square pool fires, denoted as pool A and B, were located parallel on a fireproof board (1.5 m × 0.5 m) and placed on an electronic balance. The electronic balance was XA32001L series manufactured by Mettler Toledo® Ltd (maximum load 34 kg, precision 0.1 g, sampling interval 1 s). Based on Ref. [10], four pool side lengths (D) of 8, 10, 13 and 16 cm were used to

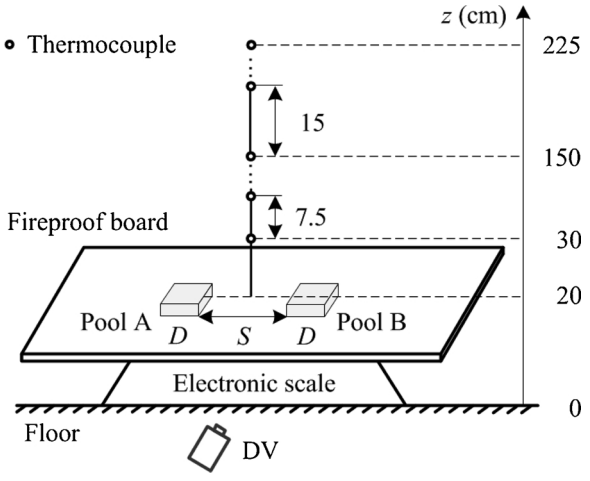

Fig. 1. Experimental setup.

ensure the pool fire is outside the conduction dominated regime. The pools were 4 cm deep and heptane was used as the fuel with an initial depth of 1.5 cm. Preliminary tests with different initial fuel depths of 1.0 cm, 1.5 cm and 2.0 cm were conducted. Taking the case of $D = 16$ cm and $S = 0$ cm as an example, the total mass loss rate against time for the three initial fuel depths is presented in Fig. 2. To illustrate the steady burning time, taking a certain mass loss rate value of 3 g/s as the criterion, it is regarded that the steady burning begins at the time of mass loss rate arriving at 3 g/s and it ends at the time of mass loss rate decreasing to 3 g/s and following a trend of decline. Note that even though the criterion of 3 g/s is a bit of subjective, the aforementioned trends also hold and the differences of average mass loss rates determined by various steady burning times are proved very small within errors of 2%. It can be observed from Fig. 2 that both the steady burning time and the burn out time of pools increase with increasing the fuel depth, while the average mass loss rates at the steady state under the three initial fuel depths are nearly identical. The above findings suggest that the fuel burning during the steady stage arrives at a balance between the fuel evaporation and the heat feedback received by fuel. And the balance is weakly affected by the initial fuel depth. Therefore, the initial fuel depth of 1.5 cm was selected to investigate the effect of heat feedback on burning rate at the steady state as it can provide sufficient steady burning time and the impact of conduction of pool rims on burning is insignificant. The pool edge spacing (S) was varied from zero to several times of $D/2$, as listed in Table 1. For comparison, the cases with pool A burning individually were also conducted.

As shown in Fig. 1, a column of 14 thermocouples with two intervals of 7.5 cm from 30 cm to 150 cm high and 15 cm from 150 cm to 225 cm high was positioned at the center of the two pools. The thermocouples were K-type with the diameter of 1 mm. A digital Sony camera (HDR-CX900) with spatial resolution of 1920 × 1080 and frame rates of 50 fps was employed to record the flame shape from the front view. It should be noted that the heat fluxes around the flames were also measured during experiments. As the heat flux is not the scope of this work, it is not presented here. The ambient temperature and humidity during experiments were about 303 K and 65%, respectively. Each experiment was repeated two times. The calculated maximum standard deviations of mass burning rate and flame height were respective no more than 0.04 g/s and 5 cm, which shows good repeatability. It is assumed that the two pools have identical flame shapes and burning rates, and the average data at the steady state were used in the following. A detailed uncertainty analysis was carried out to estimate the uncertainty of measurements, as presented in Appendix A. It was found that the maximum uncertainties in the burning rate, flame height and temperature are approximately ± 4.2%, ± 4.9% and ± 3.3%, respectively.

3. Results and discussion

3.1. Flame shape

3.1.1. Flame merging behaviors

Taking the pools of $D = 13$ cm as an example, the typical flame images during steady state with increasing spacing are shown in Fig. 3. It is observed that the flame shape can be divided into three regions: fully merging region when $0 \le S/D \le 2$, intermittent merging region when $2 < S/D \le 4$ and fully separating region when $S/D > 4$. The same trend can be found for the other three pool sizes of 8, 10 and 16 cm.

3.1.2. Flame height

The mean flame height above the pool surface (L_f) with an intermittency (I_f) of 0.5 as proposed by Zukoski et al. [26] was determined in this work by using the image processing method [21,27]. For the merging cases, the whole flame height of two flames is the merged flame height, while for the non-merging cases, the averaged flame height of two flames is determined as the flame height. Fig. 4 shows the measured flame heights under various S and D. It is observed that as the as S/D decreases, L_f increases first until it reaches the peak value at about $S/D = 0.5$–1 and then decreases slightly until $S/D = 0$.

In our former study [21], a theoretical analysis was conducted to study the effect of air entrainment on flame height of two propane gas fires. The region between the two fires is denoted as the additional entrainment region. The mass transfer among the flame region, additional entrainment region and surrounding ambient region was evaluated using Bernoulli's theory. By introducing a parameter λ characterizing the relationship between free air entrainment rates under zero spacing and spacing higher than zero, the flame height of two fires with non-zero spacing ($L_{f,S>0}$) can be expressed as [21]

$$\frac{L_{f,S>0}}{L_{f,S=0}} = \frac{6D(1+\lambda)}{6D + 2S/\sqrt{1 + (\Delta T_{add}/T_\infty + 1)(S/D)^2}} \quad (1)$$

where $L_{f,S=0}$ is the flame height with zero spacing, ΔT_{add} is the temperature rise in the additional region, T_∞ is the ambient temperature.

Logically, the same derivation process can be applied for two pool fires. Hence Eq. (1) is adopted to estimate the flame height in this work. To develop an general correlation of $L_{f,S>0}$, the determination of $\Delta T_{add}/T_\infty$ and λ are required. For two gas burners in Ref. [21],

$$\Delta T_{add}/T_\infty = f(\dot{Q}, D, S) \quad (2a)$$

$$\lambda = f(\dot{Q}, D) \quad (2b)$$

where $\dot{Q}$ is the heat release rate of each burner (HRR). As the flame height of gas burners is mainly controlled by the air entrainment and largely dependent on the fuel supply rate, both $\Delta T_{add}/T_\infty$ and λ are functions of $\dot{Q}$, as shown in Eq. (2a) and (2b). Unlike the gas fires, the burning rate and the resulting $\dot{Q}$ of pool fires are significantly affected by the pool size and spacing. Therefore, Eq. (2a) and (2b) can be simplified as

$$\Delta T_{add}/T_\infty = f(D, S) \quad (3a)$$

$$\lambda = f(D, S) \quad (3b)$$

Compared to Eq. (2a) and (2b), the impact of $\dot{Q}$ on $\Delta T_{add}/T_\infty$ and λ is implicitly embedded in D and S. The expression of $\Delta T_{add}/T_\infty$ can be determined experimentally. It is found that the measured temperature at the vertical centerline between two pools increases and then decreases with increasing height. The region with increasing temperatures is treated as the additional region (see Fig. 5), the ΔT_{add} is determined as the average temperature rises within this region. The radiation correction is performed for the measured temperatures using the method reported in Ref. [28]. Fig. 5 shows the corrected $\Delta T_{add}/T_\infty$ against S/D. It is seen that $\Delta T_{add}/T_\infty$ decreases as the S/D increases while it is

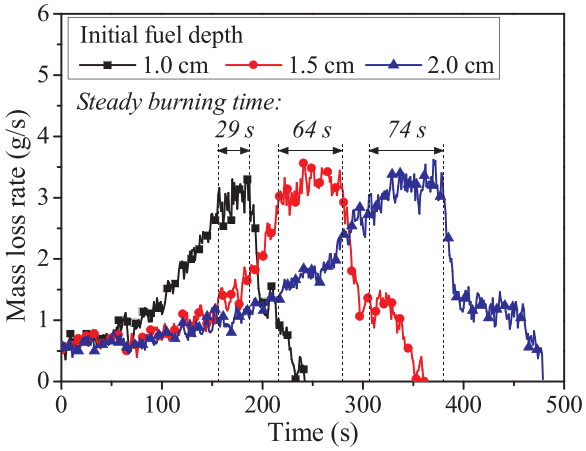

Fig. 2. Total mass loss rate against time under different initial fuel depths ($D = 16$ cm, $S = 0$ cm).

Table 1
Experimental details.

Test condition	Pool side length D (cm)	Normalized spacing S/D
Two fires	8	0, 0.5, 1, 1.5, 2, 2.5, 3, 4, 5, 6
	10	0, 0.5, 1, 1.5, 2, 3, 4, 5, 6
	13	0, 0.5, 1, 1.5, 2, 3, 4, 5
	16	0, 1, 2, 3, 4, 5
One fire	8, 10, 13, 16	–

weakly affected by D. Fitting the data points gives

$$\Delta T_{add}/T_\infty = 3.95\exp(-0.43S/D) \quad (4)$$

From Eq. (4), when S/D increases to 16, $\Delta T_{add}/T_\infty \approx 0.004$ and $\Delta T_{add} < 1$ K. The very low temperature rise in the additional region suggests that the pool fires have completely separated with no interaction when $S/D \geq 16$.

Substituting $\Delta T_{add}/T_\infty$, $L_{f,S>0}$ and $L_{f,S=0}$ into Eq. (1), the relationship between calculated λ and S/D is plotted in Fig. 6. It can be seen that λ decreases with increasing S/D. Up to infinite S, Eq. (1) can be simplified as

$$L_{f,SF}/L_{f,S=0} = 3/4(1+\lambda) \quad (5)$$

where $L_{f,SF}$ is the flame height of single fire. The values of λ for singe fires can be calculated using Eq. (5) of which the average value is −0.13. Substituting $\lambda = -0.13$ into Eq. (5) gives $L_{f,SF}/L_{f,S=0} = 0.65$, suggesting that the flame height of single square fire is 0.65 times of the two fires with zero spacing. It is worth noting that the constant 0.65 is quite consistent with the 0.63 proposed by Sugawa and Takahashi [20]. Taking $\lambda = -0.13$ as the lower limit to fit the data points in Fig. 6 gives:

$$\lambda = -0.13 + 0.21(S/D)^{-0.47} \quad (6)$$

Substituting Eqs. (4) and (6) into Eq. (1) and taking $L_{f,S=0}$ into account, the final expression of flame height is formulated as:

$$\frac{L_{f,S}}{L_{f,S=0}} = \begin{cases} 1, & S = 0 \\ \dfrac{3\left(0.87 + 0.21\left(\frac{S}{D}\right)^{-0.47}\right)}{3 + \left(\frac{S}{D}\right)/\sqrt{1 + \left(3.95\exp\left(-0.43\frac{S}{D}\right) + 1\right)\left(\frac{S}{D}\right)^2}}, & S > 0 \end{cases} \quad (7)$$

Eq. (7) indicates that the flame height ($L_{f,S}$) of two identical square pool fires can be determined using $L_{f,S=0}$ and S/D. It should be noted that for the cases of non-zero spacing, $L_{f,SF}/L_{f,S=0} = 0.65$ determines $L_{f,S=0} = 1.54L_{f,SF}$. The flame height of single fire can be calculated using the Heskestad's model [29], $L_{f,SF} = 0.235\dot{Q}^{2/5} - 1.02D$, which is also validated by the single fire cases in this work. As a result, the effect of heat release rate is implicitly embodied in Eq. (7). It should be recognized that the combustion efficiency will mainly affect the heat release rate. Weng et al. [8] experimentally measured the combustion efficiency of multiple wood crib fires in free space. They found that for the fire array 2 by 2, the ratio of combustion efficiencies between the merged flame (fire spacings of 0–5 cm) and the single fire is within 0.94–1.09. Based on the comparable combustion efficiencies between 4 fires and one fire, it is reasonable to suppose that the combustion efficiency of the present two square pool fires is close to the single fire. Therefore, the effect of combustion efficiency is believed to be small. In spite of this, an additional advantage of Eq. (7) is that it can avoid determining the combustion efficiency of two interacting pool fires.

For validation, the calculated flame heights using Eq. (7) are

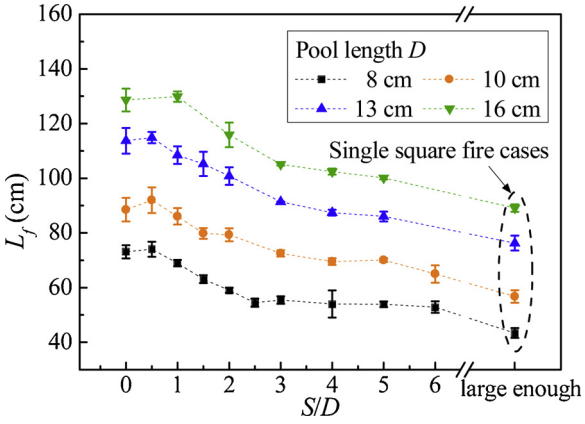

Fig. 4. Measured flame height (L_f) versus S/D.

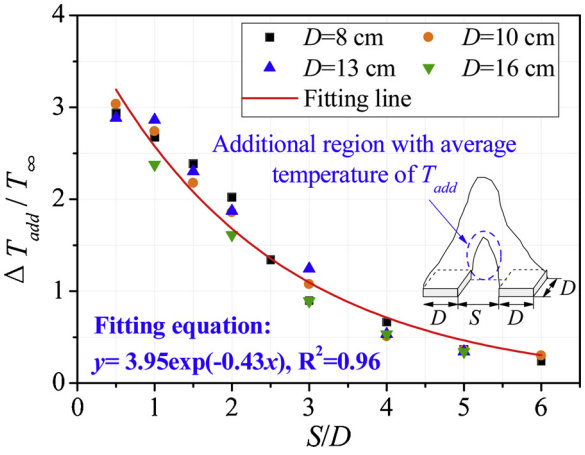

Fig. 5. Correlation of $\Delta T_{add}/T_\infty$ and S/D.

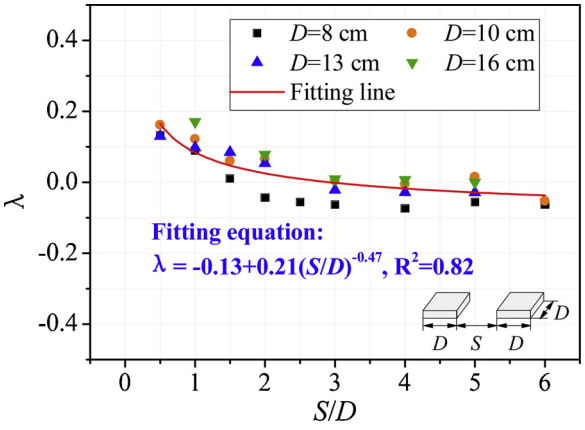

Fig. 6. Relationship between the calculated λ using Eq. (1) and S/D.

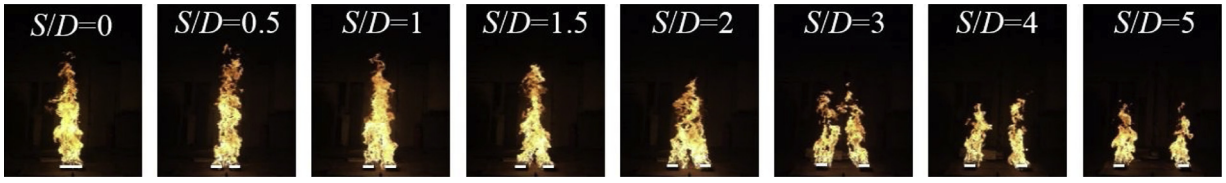

Fig. 3. Snapshots of flame shape with increasing S under D = 13 cm.

compared to the previous studies [17–21]. Fan and Tang [17] experimentally obtained the flame heights of two square heptane pool fires with $D = 7$ and 10 cm and $S = 0$–40 cm. The flame height data from two heptane pool fires with diameters (D) of 10, 20 and 40 cm and $S = 0$–$6D$ were reported by Li and Liu [18]. Vasanth et al. [19] numerically studied the flame heights of two circular heptane pool fires with $D = 4.8$, 6.8 and 8.3 cm and $S = 0.25D$–$1.08D$. Other than the liquid fuel, Sugawa and Takahashi [20] measured the flame heights of two rectangular propane gas burners with burner sizes of $40(W) \times 2(D)$ cm^2 and 80×2 cm^2. The long edges of the burners were parallel and S was varied from 0 to 30 cm. Wan et al. [21] measured the flame heights of two square propane gas burners with $D = 15$ cm and $S = 0$–$4D$. Fig. 7 shows the comparison of calculated and measured flame heights both in this work and literatures. It is observed that the calculated flame heights agree well with the experimental results, suggesting that Eq. (7) is reliable in predicting the flame height of two identical heptane and propane fires in open space.

3.2. Mass burning rate

Fig. 8 shows the time-averaged burning rate per unit area of each pool ($\dot{m}''$) against S/D at steady state. There is no surprising that $\dot{m}''$ changes non-monotonically with S, as observed by the former studies [9,13]. Next, we attempt to quantify the burning rate of two interacting fires from the view of heat feedback mechanism.

At the steady state, the energy balance at the fuel surface can be expressed as [30]:

$$\dot{m}''\Delta H_g = \dot{q}_c'' + \dot{q}_r'' \tag{8}$$

where ΔH_g is the heat of gasification, $\dot{q}_c''$ and $\dot{q}_r''$ are the convective and radiative heat fluxes received by the pool, respectively. The conductive heat transfer is ignored in Eq. (8) based on the following reasons. For the present pool size, the equivalent pool diameters with the same surface area are calculated within 9–25.5 cm, which falls in the regime where the heat feedback is dominated by convection and/or radiation based on the four regimes divided by Hottel [10]. Vali et al. [31] experimentally studied the energy transfer of a circular methanol pool fire with a diameter of 9 cm under three different fuel depths of 6 mm, 12 mm and 18 mm. They revealed that for the overall three fuel depths, the average portions of the conductive, convective and radiative heat transfers to the fuel surface are 22%, 75% and 3%, respectively. Their study indicates that the convective heat transfer is dominant for the pool diameter of 9 cm. Due to the low level of soot production and nonluminous flame of the methanol pool fire, the radiative heat feedback is insignificant. While for the present heptane pool fire with high soot production and luminous flame, the radiative heat feedback is deemed larger than that of the methanol pool fire with with the same pool size. And the radiative heat feedback would increase with increasing the pool size. Therefore, the conductive heat feedback is ignored in this work because of the pool diameters of 9–25.5 cm.

Fig. 9 shows the schematic diagram of the flame heat feedback to the fuel surface under different fire numbers. For a single fire (Fig. 9a), Eq. (8) can be specified as

$$\dot{m}_{SF}''\Delta H_g = \dot{q}_{c,SF}'' + \dot{q}_{r,SF}'' \tag{9}$$

For two interacting fires (Fig. 9b), the heat feedback to one of the pools (labelled as pool A for convenience in the following) is given by

$$\dot{m}_{MF,A}''\Delta H_g = \dot{q}_{c,MF-A}'' + \dot{q}_{r,MF-A}'' = \dot{q}_{c,MF-A}'' + \dot{q}_{r,A-A}'' + \dot{q}_{r,B-A}'' \tag{10}$$

where the subscripts SF and MF denote the single and multiple fires, respectively, $\dot{q}_{r,A-A}''$ is the radiation received by pool A from its own flame, $\dot{q}_{r,B-A}''$ is the flame radiation emitted by pool B and then received by pool A.

The convective heat feedback can be expressed as $\dot{q}_c'' = h(T_f - T_\infty)$ [9], where h is the convective heat transfer coefficient and T_f is the flame temperature. For the single fire cases, Ditch et al. [32] measured the $\dot{m}_{SF}''$ of circular pool fires with $D = 10$–100 cm using various fuels including heptane. Modak and Croce [30] measured the $\dot{m}_{SF}''$ of square PMMA pool fires with $D = 2.5$–122 cm. In these studies, the convection was recognized as the primary heat transfer mechanism for small pools and assumed as a constant for all pool sizes. The convective coefficient h is largely dependent on the flow conditions including the flame temperature (T_f) and flow velocity (U_f). For the present two fires, it found that the vertical temperature distributions for $S \to \infty$ (single square fire) and $S = 0$ are nearly identical based on the measurement temperatures at the centerline, thus the flame temperatures are very close. Hence T_f is assumed unchanged with D and S for simplification. The values of λ calculated by Eq. (6) are ranged from -0.13 to 0.16, resulting in the ratio of flow velocities $U_{f,S=0}/U_{f,S>0}$ ranging from 0.87 to 1.17. The velocity ratio being close to 1 makes it possible to assume h is weakly affected by S. Therefore, the convective heat feedback received by each pool in this work is regarded as a constant regardless of S, i.e. $\dot{q}_{c,SF}'' = \dot{q}_{c,MF-A}''$. Combining Eqs. (9) and (10), the burning rate increment can be expressed as

$$\Delta\dot{m}_A'' = \dot{m}_{MF,A}'' - \dot{m}_{SF}'' = \frac{\dot{q}_{r,A-A}'' + \dot{q}_{r,B-A}'' - \dot{q}_{r,SF}''}{\Delta H_g} \tag{11}$$

The flame radiation terms in Eq. (11) are given by:

$$\dot{q}_{r,SF}'' = \varepsilon_{SF}\sigma(T_f^4 - T_\infty^4),\ \dot{q}_{r,A-A}'' = \varepsilon_{MF}\sigma(T_f^4 - T_\infty^4),\ \dot{q}_{r,B-A}'' = F\varepsilon_{MF}\sigma(T_f^4 - T_\infty^4) \tag{12}$$

where ε is the flame emissivity, σ is the Stephan-Boltzmann constant, F is the view factor between the surface of pool A and the flame area of pool B. Substituting Eq. (12) into Eq. (11) and ignoring the constant terms yield

$$\dot{m}_{MF,A}'' - \dot{m}_{SF}'' \propto \varepsilon_{MF} + F\varepsilon_{MF} - \varepsilon_{SF} \tag{13}$$

From Eq. (13), the flame emissivity ε and view factor F ought to be determined to develop a general correlation of burning rate. Basically, the total radiative energy from a flame can be expressed as

$$\chi_{rad}\dot{m}\Delta H_c = A_f\varepsilon\sigma T_f^4 \tag{14}$$

where χ_{rad} is the flame radiative fraction, ΔH_c is the heat of combustion, A_f is the flame surface area. For fuels producing sooty flames, the radiative energy is generally accounted for 0.2–0.4 times the total HRR [33]. Specifically, Gore et al. [11] reported that χ_{rad} were approximately 0.3 for heptane pool fires with diameters of 4.6–30 cm. Similar χ_{rad} was reported by Koseki and Yumoto [12] for heptane pool fires with diameters of 30 and 60 cm. Therefore, in this work the χ_{rad} is assumed as a constant. Further assuming the flame shape is a cuboid [28] with the square base of $D \times D$ and the height of L_f, A_f

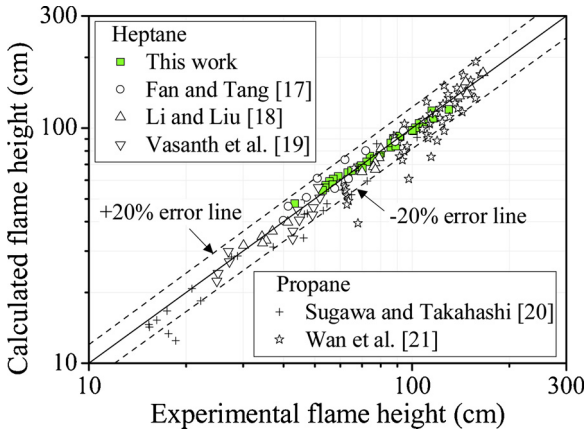

Fig. 7. Comparison of calculated and experimental flame heights.

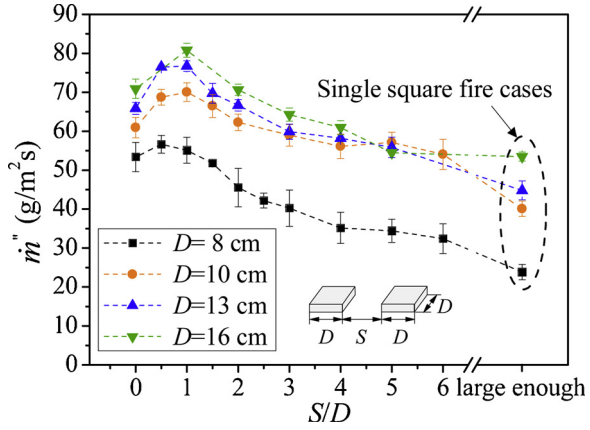

Fig. 8. Mass burning rate of each pool versus S/D.

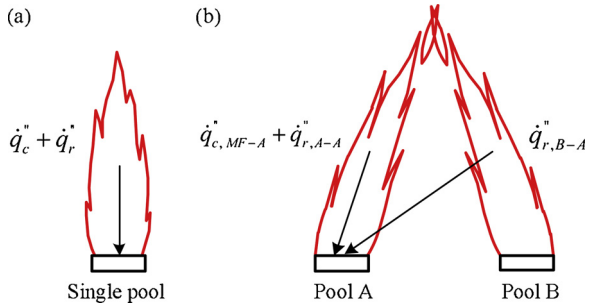

Fig. 9. Schematic diagram of the flame heat feedback received by the fuel surface of (a) single pool and (b) one of the two pools.

$= D^2 + 4DL_f \approx 4DL_f$. Eq. (14) is converted to

$$\varepsilon \propto \frac{\dot{m}}{A_f} \propto \dot{m}'' \frac{D}{L_f} \tag{15}$$

Substituting Eq. (15) into Eq. (13) gives

$$\dot{m}''_{MF,A} - \dot{m}''_{SF} \propto \dot{m}''_{MF,A}(1+F)\frac{D}{L_{f,MF}} - \dot{m}''_{SF}\frac{D}{L_{f,SF}} \tag{16}$$

It is extremely challenging in estimating the view factor between two finite areas. Assumptions have to be made to simplify the problem. Since the pool surface area is small compared to the flame area, F is modeled as the view factor between a differential area and a finite area. For simplicity, the influence of flame tilt due to the fire interaction is ignored, then the view factor between a cuboid with the dimension of $D \times D \times L_{f,MF}$ and a horizontal target is given by [28]:

$$\pi F = \tan^{-1}\frac{D}{2a} - \frac{a}{\sqrt{a^2+L_{f,MF}^2}}\tan^{-1}\frac{D}{2\sqrt{a^2+L_{f,MF}^2}} \tag{17}$$

where $a = S + D/2$. As D is much smaller than $L_{f,MF}$, $\tan^{-1}\frac{D}{2\sqrt{a^2+L_{f,MF}^2}} \approx \frac{D}{2\sqrt{a^2+L_{f,MF}^2}}$, then Eq. (17) can be simplified as

$$\pi F = \tan^{-1}\left(\frac{D}{2S+D}\right) - \frac{(2S+D)D}{(2S+D)^2+4L_{f,MF}^2} \tag{18}$$

Substituting Eq. (18) into Eq. (16) and based on the experimental data, the calculated results in Eq. (16) is plotted in Fig. 10.

It can be seen that the scatter data points from various pool sizes are now converged. Fitting the data points linearly gives

$$\dot{m}''_{MF,A} - \dot{m}''_{SF} = 12.8\left[\dot{m}''_{MF,A}(1+F)\frac{D}{L_{f,MF}} - \dot{m}''_{SF}\frac{D}{L_{f,SF}}\right] \tag{19}$$

Eq. (19) can be rearranged as:

$$\frac{\dot{m}''_{MF,A}}{\dot{m}''_{SF}} = \frac{1 - 12.8D/L_{f,SF}}{1 - 12.8(1+F)D/L_{f,MF}} \tag{20}$$

Based on $F = f(D, S, L_{f,MF})$ in Eq. (18), $L_{f,MF} = f(D, S, L_{f,S=0})$ in Eq. (7), and $L_{f,S=0} = f(L_{f,SF})$ in Eq. (5), it is deduced from Eq. (20) that the $\dot{m}''_{MF,A}$ can be predicted using the D, S, $\dot{m}''_{SF}$ and $L_{f,SF}$. To validate the proposed equation, the calculated burning rates are compared to the experimental data of two heptane pool fires from Fan and Tang [17] and Li and Liu [18], as shown in Fig. 11. It is observed that the calculated burning rates agree well with the experimental results, suggesting that Eq. (20) can be reliable in predicting the burning rate of two identical pool fires in open space. As the air entrainment and heat feedback mechanisms of multiple pool fires in a circular or square array will be different from the present two fires in a parallel array, the experimental data of Huffman et al. [9] and Liu et al. [13–15] are not presented here to compare with the proposed model.

It should be noted that the total mass of two fires was measured in the experiments, the effect of lip height (distance between the fuel surface and the top of the pool) on fire number is not considered in the original design of experiments. Babrauskas [34] stated that the steady burning of pool fire would reach if the fuel layer is large enough until the boilover occurred. Koseki et al. [35] indicated that a hot zone of at least 5–10 mm layer thickness is necessary for boilover. Using circular pools in diameters of 0.3–3.05 m and fuel thicknesses of 1–10 cm, Koseki et al. [35] further found that the variation of lip height has a little impact on the burning rate. In the latter study performed by Chatris et al. [36] on the burning rate of circular pools in diameters of 1.5–4 m and lip heights of 20–40 cm (fuel thickness maintained at 1 cm), they also found that the burning rate is weakly affected by the lip height. Both of them attributed this weak effect to the thin fuel layers used in their experiments. Besides, only when the fuel level is allowed to run down in the pool significantly, the burning rate would change progressively with the lip height [34]. As the thin fuel thickness of 1.5 cm is adopted in this work, the effect of lip light on the present burning rate of two fires is believed to be small regardless of the fire number.

4. Conclusions

A series of experiments was performed in open space to study the flame height and mass burning rate of two identical square pool fires. The pool size (D) and edge spacing (S) were changed. The main conclusions are:

(1) The flame shape presents three regions with increasing S: fully merging region when $0 \le S/D \le 2$, intermittent merging region when $2 < S/D \le 4$ and fully separating region when $S/D > 4$.

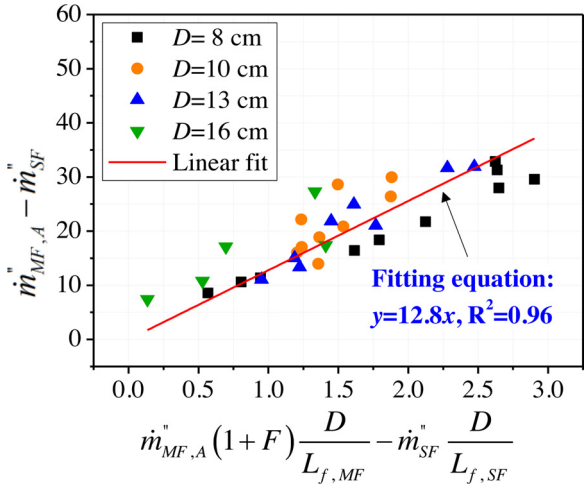

Fig. 10. Correlation of burning rate increment.

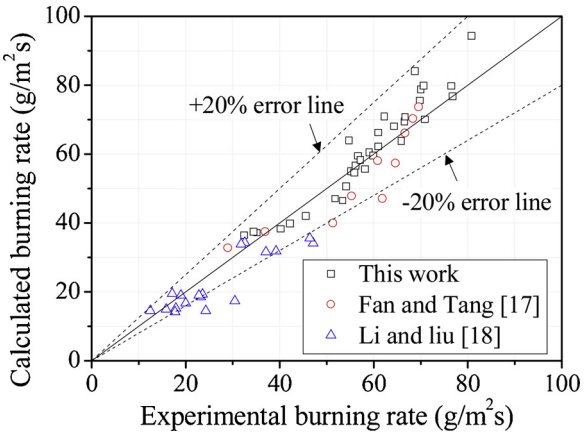

Fig. 11. Comparison of calculated and experimental mass burning rates for two pool fires.

Both the flame height and the burning rate change non-monotonically with increasing S and the peak values occur at S/D = 0.5–1.

(2) Taking the effect of air entrainment into account, a correlation for the flame height of two fires (Eq. (7)) is developed by taking into account the flame height of zero spacing ($L_{f,S=0}$) and S/D. And the effect of heat release rate is implicitly embodied in $L_{f,S=0}$. The comparison with experimental results shows that the proposed equation is suitable for predicting the flame heights of two identical heptane and propane fires. An additional advantage of the proposed model for flame height is that it can avoid determining the combustion efficiency of two interacting pool fires.

(3) Based on the energy balance at the pool surface, a theoretical correlation for predicting the burning rate is developed. The proposed correlation (Eq. (20)) indicates that the burning rate of one of the two fires can be predicted using the burning rate and flame height of the single fire and the pool size and spacing. The correlation is also validated using the experimental and literature data, which presents a reasonable reliability.

The results presented here would help better understanding the physical mechanism of interacting fires and provide viable models to determine the flame height and burning rate of two identical pool fires. The flame outward radiation and the resulting possibility of fire ignition can be further studied, which can give a guidance of the fire safety distance between discrete combustibles. It should be recognized that the air entrainment and heat feedback mechanisms of two pool fires with different dimensions will be different from that of the two identical fires. As a result, the present models for burning rate and flame height might be unsuitable. It is significant to reveal the burning behaviors of two pool fires with different sizes, which will be studied in the near future.

Acknowledgements

This work was supported by National Natural Science Foundation of China (NSFC, Grant No. 51722605), the National Post-doctoral Program for Innovative Talents (Grant No. BX20180288). Jie Ji was supported by the National Program for Support of Top-Notch Young Professionals and the Youth Innovation Promotion Association of CAS (2015386).

Appendix A. Uncertainty analysis

The uncertainty analysis for the measurements of burning rate, flame height and temperature is adapted from the method of Wheeler and Ganji [37]. Given a result R, which is a function of n measured independent variables, x_1, x_2 …, x_n,

$$R = f(x_1, x_2 \ldots, x_n) \tag{A1}$$

Based on the principle of propagation of uncertainty, the absolute uncertainty of R, δR can be estimated by a root sum square method [37]:

$$\delta R = \left\{ \sum_{i=1}^{n} \left(\frac{\partial R}{\partial x_i} \delta x_i \right)^2 \right\}^{1/2} \tag{A2}$$

where δx_i is the absolute uncertainty of the measured variable x_i.

If R can be calculated in a pure product form of the measured values [37]:

$$R = C x_1^a x_2^b x_3^c \cdots x_n^N \tag{A3}$$

The relative uncertainty of R, $\frac{\delta R}{R}$ can be expressed as [37]:

$$\frac{\delta R}{R} = \left[\left(a \frac{\delta x_1}{x_1} \right)^2 + \left(b \frac{\delta x_2}{x_2} \right)^2 + \cdots + \left(N \frac{\delta x_n}{x_n} \right)^2 \right]^{1/2} \tag{A4}$$

Based on Eq. (A4), the uncertainty of measurements in this work can be estimated in the following.

(1) Uncertainty of the burning rate measurement

The uncertainty of the burning rate measurement is referred to the study of Shafee and Yozgatligil [38]. The mass burning rate per unit area of pool can be calculated as:

$$\dot{m}'' = \frac{\Delta m}{\Delta t \cdot A} \tag{A5}$$

where Δm is the mass loss, Δt is the time interval, A is the pool surface area.

Similar to Eq. (A2), the uncertainty of the burning rate measurement can be determined as

$$\delta \dot{m}'' = \pm \left[\left(\frac{\partial \dot{m}''}{\partial \Delta m} \delta \Delta m \right)^2 + \left(\frac{\partial \dot{m}''}{\partial \Delta t} \delta \Delta t \right)^2 + \left(\frac{\partial \dot{m}''}{\partial A} \delta A \right)^2 \right]^{1/2} \tag{A6}$$

where $\frac{\partial \dot{m}''}{\partial \Delta m} = \frac{1}{\Delta t \cdot A}$, $\frac{\partial \dot{m}''}{\partial \Delta t} = \frac{-\Delta m}{(\Delta t)^2 \cdot A}$, $\frac{\partial \dot{m}''}{\partial A} = \frac{-\Delta m}{\Delta t \cdot A^2}$.

Based on Eq. (A6), the relative uncertainty of measured burning rate, $\frac{\delta \dot{m}''}{\dot{m}''}$ can be obtained

$$\frac{\delta \dot{m}''}{\dot{m}''} = \pm\left[\left(\frac{\Delta m}{\dot{m}''}\frac{\partial \dot{m}''}{\partial \Delta m}\frac{\delta \Delta m}{\Delta m}\right)^2 + \left(\frac{\Delta t}{\dot{m}''}\frac{\partial \dot{m}''}{\partial \Delta t}\frac{\delta \Delta t}{\Delta t}\right)^2 + \left(\frac{A}{\dot{m}''}\frac{\partial \dot{m}''}{\partial A}\frac{\delta A}{A}\right)^2\right]^{1/2} \tag{A7}$$

where $\frac{\delta \Delta m}{\Delta m}$, $\frac{\delta \Delta t}{\Delta t}$ and $\frac{\delta A}{A}$ are relative uncertainties of the measured mass loss, time interval in the steady stage and pool surface area, respectively.

The uncertainty of fuel mass measurement depends on the balance readability, linearity, and repeatability [38], all of them were ± 0.1 g as provided in the technical guide of the electronic balance. The uncertainties of time interval and pool surface area were determined based on the load cell resolution of ± 0.2 s and the ruler resolution of ± 1 mm, respectively. Taking these values into Eq. (A7) and considering all experimental cases, it was calculated that the maximum relatively uncertainty of the burning rate is approximately ± 4.2%.

(2) Uncertainty of the flame height measurement

In this work, the flame height was determined through image processing method developed by Yan et al. [39]. The flames were recorded by a digital camera. All images were composed of 1920 × 1080 pixels and were captured at a rate of 50 frames per second. By averaging total 3000 frames (60 s) during the steady stage, the mean flame height was then obtained. In the experiments, a target along the flame center and at a fixed height from the pool surface was used as the reference to determine the relationship between the recorded height in the unit of pixels and the actual height in the unit of meters. Then the flame height, L_f can be determined as

$$L_f = \frac{P \cdot \Delta L}{\Delta P} \tag{A8}$$

where P is the flame height in pixels, ΔL is the target height in meters, ΔP is the target height in pixels. These parameters were measured using an electronic digital caliper with a resolution of ± 1 mm.

Similarly, the uncertainty of measured flame height can be determined as

$$\delta L_f = \pm\left[\left(\frac{\partial L_f}{\partial P}\delta P\right)^2 + \left(\frac{\partial L_f}{\partial \Delta L}\delta \Delta L\right)^2 + \left(\frac{\partial L_f}{\partial \Delta P}\delta \Delta P\right)^2\right]^{1/2} \tag{A9}$$

where $\frac{\partial L_f}{\partial P} = \frac{\Delta L}{\Delta P}$, $\frac{\partial L_f}{\partial \Delta L} = \frac{P}{\Delta P}$, $\frac{\partial L_f}{\partial \Delta P} = \frac{-P \cdot \Delta L}{(\Delta P)^2}$.

Based on Eq. (A9), the relative uncertainty of measured flame height, $\frac{\delta L_f}{L_f}$ can be obtained

$$\frac{\delta L_f}{L_f} = \pm\left[\left(\frac{P}{L_f}\frac{\partial L_f}{\partial P}\frac{\delta P}{P}\right)^2 + \left(\frac{\Delta L}{L_f}\frac{\partial L_f}{\partial \Delta L}\frac{\delta \Delta L}{\Delta L}\right)^2 + \left(\frac{\Delta P}{L_f}\frac{\partial L_f}{\partial \Delta P}\frac{\delta \Delta P}{\Delta P}\right)^2\right]^{1/2} \tag{A10}$$

where $\frac{\delta P}{P}$, $\frac{\delta \Delta L}{\Delta L}$ and $\frac{\delta \Delta P}{\Delta P}$ are relative uncertainties of the measured flame height in pixels, target height in meters and in pixels, respectively. Based on the resolution of electronic digital caliper, $\delta P = \pm 2$ pixels, $\delta \Delta L = \pm 1$ mm, $\delta \Delta P = \pm 2$ pixels, respectively. Taking all experimental cases into account, it was calculated that the maximum relative uncertainty of flame height measurement is about ± 4.9%.

(3) Uncertainty of the temperature measurement

Prior to the present study, Rasiah [40] performed a calibration of T-type thermocouples and conducted uncertainty analysis using the method of Wheeler and Ganji [37]. He estimated an uncertainty in temperature rise of $\delta \Delta T = \pm 0.06$ ℃. Based on the study of Rasiah, a conservative value of $\delta \Delta T = \pm 0.1$ ℃ was used by Wright et al. [41] to estimate the uncertainty of temperature. In addition, Ma [42] measured the temperature using E-type thermocouples and estimated the uncertainty of temperature as ± 1 ℃. In this work, the temperature was measured by K-type thermocouples and the uncertainty of the temperature reading was ± 0.1 ℃. A conservative value of ± 1 ℃ was considered in this work, then the relative uncertainty of temperature can be calculated as $\frac{\delta T}{T} = \pm\left(\frac{1°C}{T(°C)}\right)$. As the ambient temperature was about 30 ℃, the maximum relative uncertainty of temperature measurement was approximately ± 3.3%.

References

[1] S. Vasanth, S.M. Tauseef, T. Abbasi, S.A. Abbasi, Multiple pool fires: occurrence, simulation, modeling and management, J. Loss Prev. Process Ind. 29 (2014) 103–121, https://doi.org/10.1016/j.jlp.2014.01.005.

[2] B. Chen, S.X. Lu, C.H. Li, Q.S. Kang, V. Lecoustre, Initial fuel temperature effects on burning rate of pool fire, J. Hazard. Mater. 188 (1-3) (2011) 369–374, https://doi.org/10.1016/j.jhazmat.2011.01.122.

[3] F. Ferrero, M. Munoz, B. Kozanoglu, J. Casal, J. Arnaldos, Experimental study of thin-layer boilover in large-scale pool fires, J. Hazard. Mater. 137 (3) (2006) 1293–1302, https://doi.org/10.1016/j.jhazmat.2006.04.050.

[4] C. Wang, J. Guo, Y. Ding, J. Wen, S. Lu, Burning rate of merged pool fire on the hollow square tray, J. Hazard. Mater. 290 (2015) 78–86, https://doi.org/10.1016/j.jhazmat.2015.02.069.

[5] F. Tang, L.J. Li, K.J. Zhu, Z.W. Qiu, C.F. Tao, Experimental study and global correlation on burning rates and flame tilt characteristics of acetone pool fires under cross air flow, Int. J. Heat Mass Transf. 87 (2015) 369–375, https://doi.org/10.1016/j.ijheatmasstransfer.2015.04.019.

[6] R.M. Leite, F.R. Centeno, Effect of tank diameter on thermal behavior of gasoline and diesel storage tanks fires, J. Hazard. Mater. 342 (2018) 544–552, https://doi.org/10.1016/j.jhazmat.2017.08.052.

[7] H. Wan, Z. Gao, J. Ji, J. Fang, Y. Zhang, Experimental study on horizontal gas temperature distribution of two propane diffusion flames impinging on an unconfined ceiling, Int. J. Therm. Sci. 136 (2019) 1–8, https://doi.org/10.1016/j.ijthermalsci.2018.10.010.

[8] W. Weng, D. Kamikawa, Y. Hasemi, Experimental study on merged flame characteristics from multifire sources with wood cribs, Proc. Combust. Inst. 35 (3) (2015) 2597–2606, https://doi.org/10.1016/j.proci.2014.05.112.

[9] K. Huffman, J. Welker, C. Sliepcevich, Interaction effects of multiple pool fires, Fire Technol. 5 (3) (1969) 225–232, https://doi.org/10.1007/BF02591520.

[10] H. Hottel, Certain laws governing the diffusive burning of liquids by Blinov and Khudiakov, Fire Res. Abstr. Rev. 1 (1959) (1957) 41–44.

[11] J. Gore, M. Klassen, A. Hamins, T. Kashiwagi, Fuel property effects on burning rate and radiative transfer from liquid pool flames, Proc. 3rd International Symposium on Fire Safety Science (1991) 395–404.

[12] H. Koseki, T. Yumoto, Air entrainment and thermal radiation from heptane pool fires, Fire Technol. 24 (1) (1988) 33–47, https://doi.org/10.1007/BF01039639.

[13] N. Liu, Q. Liu, J.S. Lozano, L. Shu, L. Zhang, J. Zhu, Z. Deng, K. Satoh, Global burning rate of square fire arrays: experimental correlation and interpretation, Proc. Combust. Inst. 32 (2) (2009) 2519–2526, https://doi.org/10.1016/j.proci.2008.06.086.

[14] N. Liu, Q. Liu, Z. Deng, S. Kohyu, J. Zhu, Burn-out time data analysis on interaction effects among multiple fires in fire arrays, Proc. Combust. Inst. 31 (2) (2007) 2589–2597, https://doi.org/10.1016/j.proci.2006.08.110.

[15] N. Liu, Q. Liu, J.S. Lozano, L. Zhang, Z. Deng, B. Yao, J. Zhu, K. Satoh, Multiple fire interactions: a further investigation by burning rate data of square fire arrays, Proc. Combust. Inst. 34 (2) (2013) 2555–2564, https://doi.org/10.1016/j.proci.2012.06.098.

[16] J. Ji, H. Wan, Z. Gao, Y. Fu, J. Sun, Y. Zhang, K. Li, S. Hostikka, Experimental study on flame merging behaviors from two pool fires along the longitudinal centerline of model tunnel with natural ventilation, Combust. Flame 173 (2016) 307–318,

https://doi.org/10.1016/j.combustflame.2016.08.020.
[17] C.G. Fan, F. Tang, Flame interaction and burning characteristics of abreast liquid fuel fires with cross wind, Exp. Therm. Fluid Sci. 82 (2017) 160–165, https://doi.org/10.1016/j.expthermflusci.2016.11.010.
[18] Z. Li, N. Liu, Experimental study on combustion characteristics of multiple heptane pool fires, Fire Saf. Sci. 21 (3) (2012) 109–116, https://doi.org/10.7666/d.y2125386.
[19] S. Vasanth, S. Tauseef, T. Abbasi, A. Rangwala, S. Abbasi, Assessment of the effect of pool size on burning rates of multiple pool fires using CFD, J. Loss Prev. Process Ind. 30 (2014) 86–94, https://doi.org/10.1016/j.jlp.2014.04.011.
[20] O. Sugawa, W. Takahashi, Flame height behavior from multi-fire sources, Fire Mater. 17 (3) (1993) 111–117, https://doi.org/10.1002/fam.810170303.
[21] H. Wan, J. Ji, K. Li, X. Huang, J. Sun, Y. Zhang, Effect of air entrainment on the height of buoyant turbulent diffusion flames for two fires in open space, Proc. Combust. Inst. 36 (2) (2017) 3003–3010, https://doi.org/10.1016/j.proci.2016.07.078.
[22] C. Tao, Q. Ye, J. Wei, Q. Shi, F. Tang, Experimental study on flame–flame interaction and its merging features induced by double rectangular propane diffusion burners with various aspect ratios, Combust. Sci. Technol. (2018) 1–14, https://doi.org/10.1080/00102202.2018.1529031.
[23] H. Wan, Z. Gao, J. Ji, K. Li, J. Sun, Y. Zhang, Experimental study on ceiling gas temperature and flame performances of two buoyancy-controlled propane burners located in a tunnel, Appl. Energy 185 (2017) 573–581, https://doi.org/10.1016/j.apenergy.2016.10.131.
[24] H. Wan, Z. Gao, J. Ji, L. Wang, Y. Zhang, Experimental study on merging behaviors of two identical buoyant diffusion flames under an unconfined ceiling with varying heights, Proc. Combust. Inst. 37 (3) (2019) 3899–3907, https://doi.org/10.1016/j.proci.2018.05.154.
[25] A. Putnam, C. Speich, A model study of the interaction of multiple turbulent diffusion flames, Symp. (Int.) Combust. (1963) 867–877, https://doi.org/10.1016/S0082-0784(63)80093-4.
[26] E. Zukoski, B. Cetegen, T. Kubota, Visible structure of buoyant diffusion flames, Symp. (Int.) Combust. (1985) 361–366, https://doi.org/10.1016/S0082-0784(85)80522-1.
[27] L. Jiang, J.J. He, J.H. Sun, Sample width and thickness effects on upward flame spread over PMMA surface, J. Hazard. Mater. 342 (2018) 114–120, https://doi.org/10.1016/j.jhazmat.2017.08.022.
[28] H. Wan, Z. Gao, J. Ji, J. Sun, Y. Zhang, K. Li, Predicting heat fluxes received by horizontal targets from two buoyant turbulent diffusion flames of propane burning in still air, Combust. Flame 190 (2018) 260–269, https://doi.org/10.1016/j.combustflame.2017.12.003.
[29] G. Heskestad, Fire plumes, flame height, and air entrainment, SFPE Handbook of Fire Protection Engineering, 3rd ed., National Fire Protection Association, Quincy, Massachusetts, 2002 p. 2–3.
[30] A.T. Modak, P.A. Croce, Plastic pool fires, Combust. Flame 30 (1977) 251–265, https://doi.org/10.1016/0010-2180(77)90074-8.
[31] A. Vali, D.S. Nobes, L.W. Kostiuk, Fluid motion and energy transfer within burning liquid fuel pools of various thicknesses, Combust. Flame 162 (4) (2015) 1477–1488, https://doi.org/10.1016/j.combustflame.2014.11.013.
[32] B.D. Ditch, J.L. de Ris, T.K. Blanchat, M. Chaos, R.G. Bill, S.B. Dorofeev, Pool fires–an empirical correlation, Combust. Flame 160 (12) (2013) 2964–2974, https://doi.org/10.1016/j.combustflame.2013.06.020.
[33] J. Ji, C.G. Fan, W. Zhong, X.B. Shen, J.H. Sun, Experimental investigation on influence of different transverse fire locations on maximum smoke temperature under the tunnel ceiling, Int. J. Heat Mass Transf. 55 (17–18) (2012) 4817–4826, https://doi.org/10.1016/j.ijheatmasstransfer.2012.04.052.
[34] V. Babrauskas, Estimating large pool fire burning rates, Fire Technol. 19 (4) (1983) 251–261, https://doi.org/10.1007/BF02380810.
[35] H. Koseki, M. Kokkala, G.W. Mulholland, Experimental study of boilover in crude oil fires, Fire Saf. Sci. 3 (1991) 865–874, https://doi.org/10.3801/IAFSS.FSS.3-865.
[36] J. Chatris, E. Planas, J. Arnaldos, J. Casal, Effects of thin-layer boilover on hydrocarbon pool fires, Combust. Sci. Technol. 171 (1) (2001) 141–161, https://doi.org/10.1080/00102200108907862.
[37] A.J. Wheeler, A.R. Ganji, Introduction to Engineering Experimentation, Prentice Hall, New Jersey, 1996 p. 180–184.
[38] S. Shafee, A. Yozgatligil, An experimental study on the burning rates of interacting fires in tunnels, Fire Saf. J. 96 (2018) 115–123, https://doi.org/10.1016/j.firesaf.2018.01.004.
[39] W.G. Yan, C.J. Wang, J. Guo, One extended OTSU flame image recognition method using RGBL and stripe segmentation, Appl. Mech. Mater. 121–126 (2011) 2141–2145, https://doi.org/10.4028/www.scientific.net/AMM.121-126.2141.
[40] J. Rasiah, The Design and Calibration of a Thermopile for the Guarded Heater Plate Apparatus, UW 1A Electrical Engineering Work Report, University of Waterloo, Canada, 2003.
[41] J.L. Wright, N.Y.T. Huang, M.R. Collins, Thermal resistance of a window with an enclosed venetian blind: guarded heater plate measurements, ASHRAE Trans. 2 (2006) 13–21 http://hdl.handle.net/10012/11573.
[42] H. Ma, Thermal Modeling of Shape Memory Alloy Wire Actuators for Automotive Applications, PhD thesis, University of Waterloo, Canada, 2010http://hdl.handle.net/10012/5349.